The Effects of Temporally Changing Sources on Fourier Transform Spectrometers

Herbert J. Mitchell, Terrance H. Hemmer, Paul E. Lewis, Carl Salvaggio
Spectral Information Technology Applications Center[a]

ABSTRACT

A Michelson Fourier Transform Spectrometer senses an object/material in the time domain, producing an interferogram. To produce a spectrum, the interferogram is Fourier transformed into the spectral domain. Unless filtering is applied to the interferogram, all the time changing (AC) components of the interferogram contribute to the resulting spectrum. Aperiodic signals are not easily removed from the interferogram and, when transformed, result in false spectral features. Possible sources of real-world aperiodic signals are discussed and their effects on the resulting transformed spectra are demonstrated. Mitigation and avoidance techniques for some of the more common real-world aperiodic signals are discussed.

Keywords: Fourier Transform Spectroscopy, Sensor motions, Atmospheric Irregularities, Cirrus clouds

1. INTRODUCTION

SITAC has been involved with making imaging spectral measurements for many years using dispersive imaging sensors. Use of a Michelson Fourier Transform Spectrometer (FTS) with its high-energy throughput is an excellent method to obtain high-resolution spectra of stationary materials under stable conditions. For this reason, SITAC has been exploring the use of FTS sensors for future measurements. An important fact to recognize is that motions, which cause aperiodic changes in the scene being viewed during formation of the interferogram result in amplitude changes that are not related to the position of the mirror. When this data is Fourier transformed from the time domain to the spectral domain, these amplitude changes will create false spectral features. This paper seeks to explain this process and demonstrate how motions within the scene can compromise FTS sensor data. Some simple experiments conducted by the authors illustrate these motion effects. A short discussion of motion compensation methodology is also presented.

1.1 Michelson FTS Basic Concepts

A Michelson FTS instrument utilizes a beam splitter to separate the incoming light into two beams. One of the beams goes to a fixed mirror, the other to a moving mirror. When the light beams pass back through the beam-splitter, they produce, depending on the mirror's position, a pattern of constructive and destructive interference at the detectors on the focal plane of the instrument. The detector output is the varying amplitude of the passing interference fringes as source spectral emissions go in and out of phase between the fixed mirror path and the moving mirror path. The detector output is a signal in the time domain and is called an interferogram. By accurately knowing the mirror position, the varying interference fringes sensed by the detector can be transformed from the timedomain to the spectral domain. Once this transformation has occurred, the spectrum is equivalent to that obtained by a dispersive spectrometer.

The FTS detector samples all wavelengths simultaneously in the time domain during formation of the interferogram. The spectral resolution of the FTS instrument is largely controlled by the quality and distance of the mirror motion and the rate at which the detector is sampled. FTS instruments are often chosen for spectral measurements for their high spectral resolution and their greater energy throughput. They have potential to improve signal to noise ratio (SNR) under controlled conditions through signal averaging. The improvement in S/N brought about by signal averaging is proportional to the square root of the number of scans averaged.

[a] Spectral Information Technology Applications Center, 11781 Lee Jackson Memorial Highway, Suite 400, Fairfax, VA, USA 22033-3309, Phone 703-591-8546, FAX 703-591-2437.

Algorithms for Multispectral, Hyperspectral, and Ultraspectral Imagery VII, Sylvia S. Shen, Michael R. Descour, Editors, Proceedings of SPIE Vol. 4381 (2001)

The basic premise of the FTS spectrometer is that the fringe pattern changes are all due to the movement of the mirror in one arm of the instrument. Should there be anything that causes a change in irradiance incident on the focal plane detector, a corresponding change will be seen in the interferogram from that detector. This change will be independent of mirror position and result in a false feature in the interferogram. The subsequent Fourier transformation assumes all time domain changes are related to mirror position changes, thus, when the data is transformed into the spectral domain, the brightness change becomes a spectral feature. While periodic interference can be filtered out of the interferogram, aperiodic interference cannot be removed so simply.

2. PLATFORM-INDUCED AMPLITUDE CHANGES

2.1 Platform-Induced Motions

There are many sources that can cause changes in the brightness of a detector's field-of-view during formation of the interferogram (i.e. while the mirror is scanning). An aircraft moves at typical speeds of 100 to 300 m/sec at typical altitudes of 0.5km to as much as 20km. Airborne FTS applications almost insure that there will be motion-induced signal amplitude changes during formation of interferograms. These platform-motion-induced amplitude changes will induce false spectral features in the spectrum when they are transformed from the time domain to the spectral domain.

2.1.1 FTS "Push-broom" Operation

If the FTS sensor is operated in the "push-broom" mode (see Figure 1), pixels are smeared in the forward direction at approximately the same speed rate as the aircraft is moving. The aircraft ground track will move across the earth's surface at the aircraft's velocity and will vary with the winds aloft. One can multiply the ground track velocity in m/s by the mirror scan-time in seconds to get the areal increase in ground sampling distance (GSD.) If the areal increase is an appreciable fraction of the instantaneous (or static) GSD area, then the data from that detector will be severely compromised. This amount of image motion very quickly becomes unacceptable for an FTS sensor. For this reason FTS sensors are generally not used in push-broom sensing modes. One exception, however, was the 1970-era Nimbus D satellite that used an FTS sensor with a GSD that was so large (on the order of several hundred meters on a side), that the orbital motions added only a small percentage of areal change to the GSD during the mirror scan.

Platform Motions

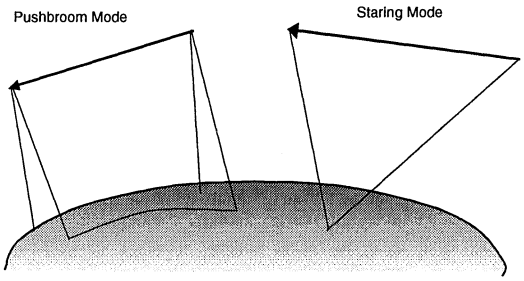

Figure 1

2.1.2 FTS "Staring" Operation

A staring sensor is one that can lock onto a point and compensate for the forward motion of the platform. This mitigates the areal change platform-induced problem, however, other motion problems as shown in Figure 2 will become significant. A staring sensor must compensate for pixel change as the platform moves toward or away from the chosen staring point. In this staring geometry, one will have to consider the drift induced by slightly imperfect aiming or imperfect stabilization. In all viewing modes, the stability of the platform is important, as any jitter or vibrations will be transformed into pixel motion on the ground.

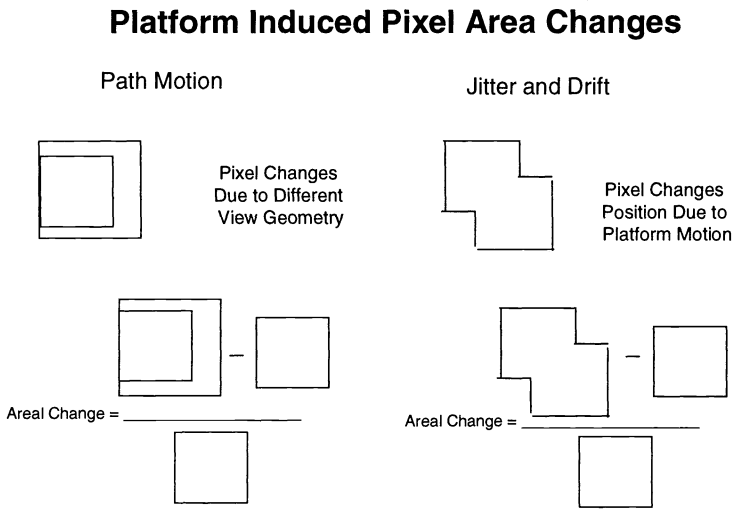

Figure 2

3. EXTERNALLY-INDUCED AMPLITUDE CHANGES

In addition to platform motions, external motions can cause amplitude changes during formation of the FTS interferogram. These external motions can be caused by the passage of cirrus, contrails, and low-water clouds in to and out of the FTS field of view during the mirror scan period. Cirrus and contrails are highly structured and can produce quite significant amplitude changes to FTS interferograms.

3.1 Clouds as External Motion Sources

Other external sources of scene motion are ice clouds, such as cirrus and contrails, and water clouds that pass through the FTS field-of-view during interferogram formation.

Ice clouds present significant external aperiodic fluctuation problems to an FTS sensor. The two most commonly encountered ice cloud forms are cirrus and contrails. There is little difference between the two ice cloud types, contrails are slightly younger and are composed of smaller particles initially. They also tend to be produced in fairly straight lines[1,2,3,4,5,6,7,8,9,10,12,13]. One might be surprised at how much of the earth can be covered by contrails. Over the United States and Europe, contrails fill as much as 2% of the total sky area[11]. Over major air routes like US-to-Europe and Japan-to-US the contrail areal coverage can be even higher.

Cirrus areal coverage is even greater than contrail coverage and exists in a great diversity of optical thickness in the visible through longwave infrared regions of the spectrum. There are many opinions as to the extent of cirrus over the earth. The canonical estimate is that at any time cirrus covers one half of the earth. Cirrus tends to be slightly more prevalent near the equator, but a study over Moscow in the early 70's claimed that it was present on 80% of the otherwise clear nights. Since the optical depth varies so much, it is hard to pin down the extent of cirrus. Laser sounding of the atmosphere is the most reliable sensing technique for cirrus detection; however, the LWIR band of the NOAA AVHRR can be used to roughly estimate the effective extent for cirrus.

Cirrus clouds can severely compromise the data taken from an airborne or space-based infrared FTS sensor. Cirrus may be structured at scale sizes far smaller than any spectral sensor GSD envisioned to date. The human eye has a resolution at cirrus altitudes of about a meter. At one meter resolution, one can readily observe both cirrus and contrail formations.

Figure 3 is a photograph of a highly structured cirrus cloud with spatial structure approaching the resolution limit of the human eye. From an aircraft, one can see even finer scales in cirrus and contrails. You can also see this fine structure by using a telescope to view cirrus and contrails from earth. Most of the time, although present, cirrus is too thin to be seen by the human eye from the ground. This sub-visible cirrus can be barely perceived using the setting or rising sun or via horizontal views out of an aircraft window. The structure properties of this sub-visual cirrus are unknown, but most probably consist of the same fine-scale structure that one can see in more dense cirrus.

Figure 3

Cirrus and contrails are composed of relatively large particles. Fresh contrail particles tend to be approximately 7 microns in diameter at a distance of 50 meters behind an aircraft. Over time they may grow to the size of a mature cirrus particle, nominally 5-10 microns in diameter and 50-150 microns in length. Air drag orients these particles so that their long axis is parallel to the earth's surface. Optically, these mature cirrus particles have an effective diameter of 25-50 microns, which is large compared to the VIS/NIR/SWIR wavelengths. As a result they are defined as geometric particles for light-scattering purposes at these wavelengths. In the LWIR, the cirrus or contrail particles fall into the Mie scattering regime, wherein the scattering of light is very efficient[13]. Therefore, in this portion of the spectrum, Mie scattering will dominate absorption and emission effects for cirrus and contrails. Rather than being dominated by a few molecular vibration bands, the emission and absorption will appear as a gray body, emitting or scattering energy over the entire LWIR region.

For an FTS sensor, cirrus clouds may produce signal at all LWIR wavelengths depending on the cloud's thickness. As the sensor flies over a cirrus cloud layer, the signal amplitude will fluctuate as a result of attenuation due to the cirrus cloud structure. If the rate of cirrus crossing is within the sampling bandwidth of the FTS detector, the cirrus structure can be transformed into false spectral features. The false spectral features may appear anywhere within the transformed spectra, the exact locations of which will be a function of cirrus structure and crossing rate encountered during interferogram formation.

Low water clouds can also introduce aperiodic fluctuation problems for an FTS sensor. Low water clouds are usually optically thick. Therefore, if a pixel's field-of-view is filled by a water cloud, nothing but the cloud will be seen. The shadows from water clouds will cool the earth, altering the upwelling and downwelling radiance field in the LWIR and

MWIR portions of the spectrum. As clouds and their shadows move through the FTS field-of-view during the formation of the interferogram, intensity changes will occur leading to false spectra. For pixels that are near a cloud edge, one must deal with the partial fill and the fact that the cloud's edge does not exhibit a sharp boundary and presents varying degrees of optical thickness.

4. TEMPORALLY CHANGING SOURCE EXPERIMENTS

4.1 Effects of Cirrus on FTS Data

For cirrus clouds exhibiting structure with a scale size on the order of 1 meter, an aircraft flying at speeds between 100 and 300 m/s with a staring sensor will cut this structure at rates of 0-300 Hz, depending on geometries and cirrus crossing angles. If cirrus structure exists at scale sizes less than 1 meter, and the aircraft is near the cirrus, the rates may be significantly higher. Additionally, the cirrus (and contrails) will be transported by the winds. Wind speeds at cirrus altitudes can be up to 100 m/s, which adds another component to the rate of cirrus interference. These approximations define a reasonable range of expected frequencies and were used as a basis for the experiments conducted by the authors.

An experiment was designed to simulate the structure/crossing rate caused by cirrus clouds and the effect it has on the formation of an interferogram. A Designs and Prototypes (D&P) microFTIR Model 102 spectrometer, sensitive from 1.5 to 50 microns, operating in the staring mode was used for this experiment. It has a mirror scan rate of 1 second and the sampling rate of its detector is 5 kHz. Ideally one could construct a device that would utilize liquid nitrogen to create cirrus particles and inject them at a few hundred to a few thousand Hz modulation rate into in an air stream that would then flow past the entrance port of the FTS instrument. Due to time and budget constraints, the authors created a simple laboratory experiment that simulated aspects of cirrus clouds using a reverse temperature contrast scenario.

The experiment utilized a cold background and a warm interference source, vice the warm earth beneath the cold cirrus interference source. For the cold background, an ice bath was used, which was stirred between measurements to keep its temperature as uniform as possible. For the warm interference source, a chopper made out of ordinary aluminum house screen was employed. The house screen provided about a 10% fill factor and was considered to be reasonably representative of moderate thickness cirrus[9]. The screen was cut into 8 segments. Four were holes and the remaining 4 segments were screen, forming a chopper blade. This chopper was fitted to a variable speed drill that could produce angular rotation up to 4000 rpm. At these rates, the chopping frequencies could be varied from 0 to 250 Hz (Figure 4).

Figure 5 shows both the measured radiance from the unobstructed ice bath as well as the radiance sensed when viewing the ice bath through the screen in a stationary position, completely filling the sensor's field-of-view. Sixteen individually derived spectra are shown for each case to demonstrate the stability of the D&P microFTIR spectrometer.

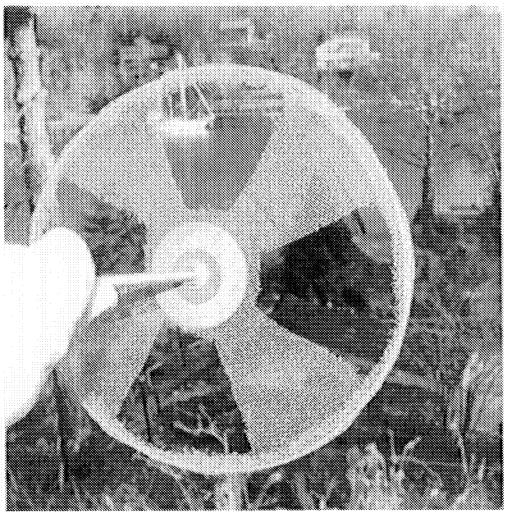

Figure 4

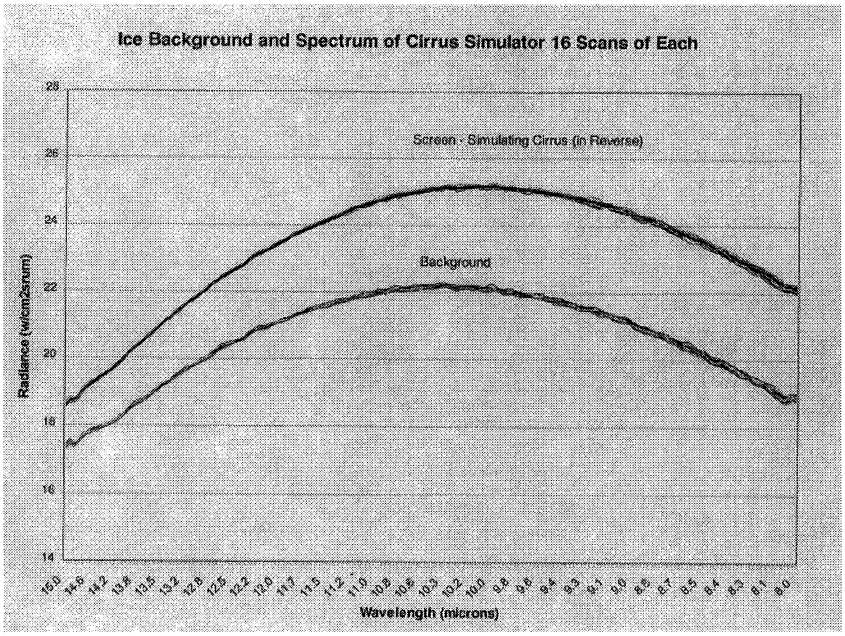

Figure 5

Figure 6 illustrates two randomly selected spectra obtained when the "cirrus simulator" was rotating through the spectrometer's field-of-view. These are typical of many such spectra and neither represents the best nor the worst of the scans. The ice bath background is also depicted. These spectra were collected with the chopper running at random speeds during the interferogram scan. Additional tests were conducted running the "cirrus simulator" at many different constant rates throughout the desired frequency range. With some practice, spectral features could be inserted anywhere within the interferometer's spectral range. This clearly should have been the result of this experiment. The magnitude of the effect on the resulting spectra exceeded the magnitude of the same effect while the screen was in a stationary position. The screen-only radiance averaged about 8% higher than the ice bath radiance. The magnitude of the spectral peaks resulting from measurements taken through the "cirrus simulator" was often twice this difference.

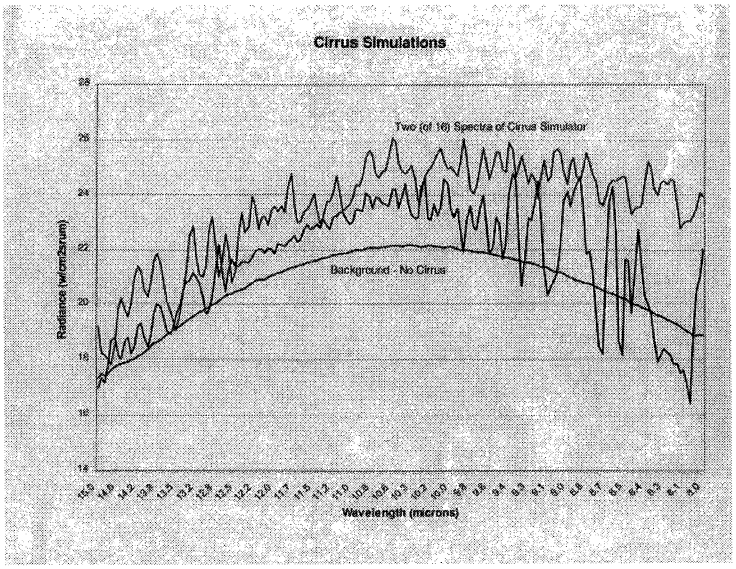

Figure 6

4.2 Effects of Jitter and Drift on FTS Data

Another experiment to illustrate the effect of platform stabilization translated into pixel motion on the ground was also conducted. To simulate the effect of pixel motion, various choppers were constructed with uneven edges. The movement of these edges simulated pixel motion on the ground caused by the platform's motion during the formation of the interferogram. Figure 7 shows two of these choppers. Again spectral features could be placed anywhere within the spectral range of the interferometer based on the frequency of this motion.

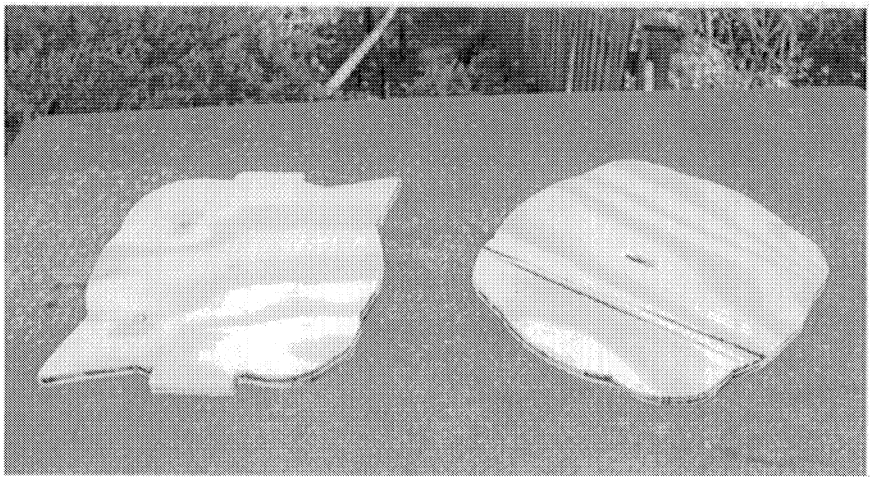

Figure 7

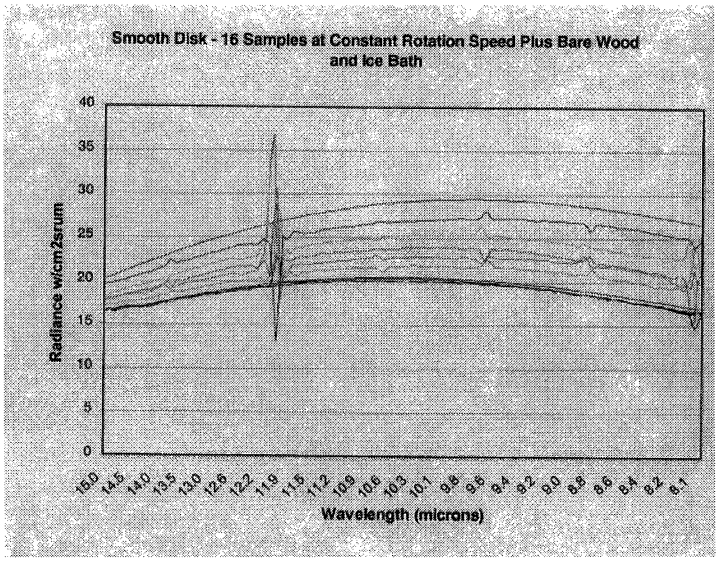

Figure 8

Figure 8 shows the result of some constant frequency runs with the same ice bath in the background. The results were as expected, amplitudes of up to twice the radiance difference observed between the ice bath and the pure chopper material when no motion is present.

5. MOTION COMPENSATION TECHNIQUES

For an imaging FTS sensor motion effects such as drift and jitter can be compensated for, as long as the motions can be correlated within the scene. Any sensor-induced motions such as drift and jitter, and the change in field-of-view due to the dynamic positioning of the platform should be correlated. In these correlated motion cases, the time dependent motion of the sensor can be estimated by measuring the positional changes of a trackable multi-pixel object (e.g. such as a building) in the detector array, at every interferogram sampling interval. The object used to estimate the motions must be sufficiently large and have sufficient two-dimensional structure so that no sub pixel positional ambiguities occur. Sub pixel positional ambiguities will result in false spectra when the interferogram is Fourier transformed. Figure 9 shows a simple hypothetical scene, which demonstrates the use of building edges to determine sensor motion during the formation of the interferogram. From these pixel position measurements, a continuous functional estimation for the apparent motions of all objects in the scene is obtained over the entire mirror scan period. As an example, for an FTS to have a 1 cm^{-1} resolution over the interval from 1400 to 700 cm^{-1} (~7-14 microns), sampling theory would require 1400 sample points. Therefore, the motion compensation function should incorporate object displacements at each of the 1400 sample points.

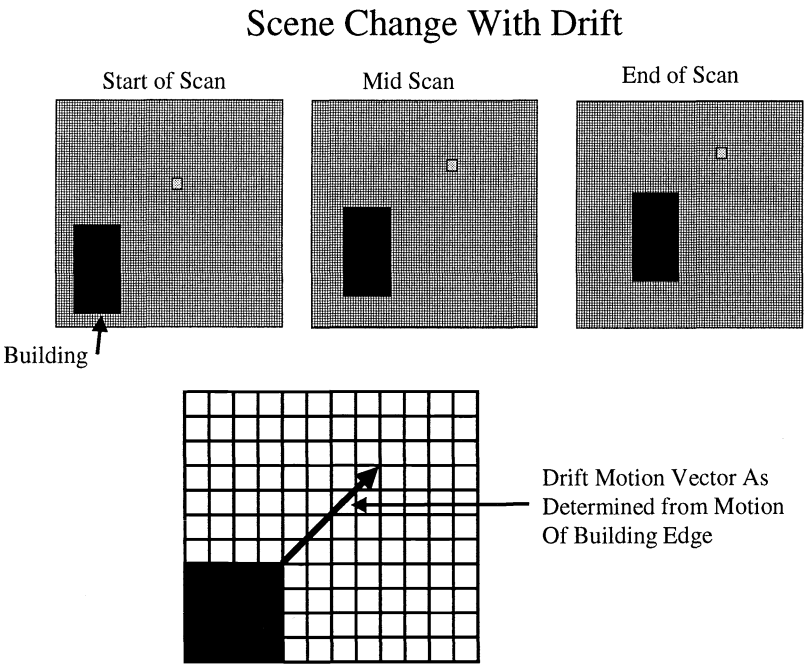

Figure 9

Once the motion function has been determined, it can be applied to the whole array of detectors to transform each pixel from the sensor platform based detector array to an Earth surface based virtual detector array. Figure 10 shows the translation vector, starting and current positions for the array as it nears the 1400th sample point. Similar position shifts will be applied to all pixels in the sensor array at each of the 1400 sample points.

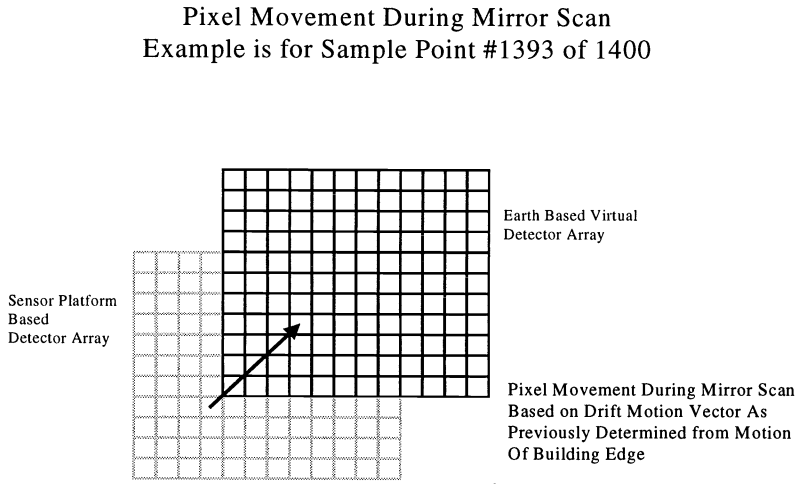

Figure 10

The motion function derived from Figures 9 and 10 can now be used to build the individual motion compensated pixels in the Earth based virtual detector array. Figure 11 shows a sequence of the motion over time. For each of the 1400 sampling increments, one must compute the overlap proportions for each platform based detector array pixel into the translated Earth based virtual detector pixel. For this example, one can see that each translated pixel at any sample point can be built up from contributions from one to four of the original pixels. This pixel shifting and assignment of proportionalities for each of the 1400 sample points becomes a formidable task for each interferogram, even for fast computers.

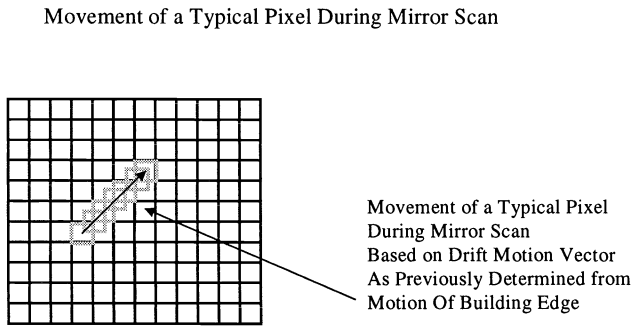

Figure 11

It must be stressed that there are several constraints when employing this type of motion compensation scheme. First, one must know the motions precisely. Any error in the motion estimates will appear as false spectral features when the interferograms are transformed. If one is dealing with a high Signal to Background (S/B) scene, such as imaging a lava flow

down the side of a mountain, the resulting spectra should not be significantly impacted by slight positional errors. However, positional errors become quite important for low S/B cases. Second, the individual detectors must be very well calibrated and their relative drifts accurately known. When one proportionally obtains interferogram information for the shifted pixels from the detector array, one must be sure that the signal has the same calibration basis. Any detector calibration differences will introduce false spectral features in the Fourier transformed interferogram. Third, the resampling of interferogram data to form the new, earth surface referenced cube effectively increases the Ground Sample Distance (GSD) of the sensor (e.g., in the illustrated case, by a factor of about four.) This may lead to lower signal-to-noise ratios and increased dependence on motion and calibration precision.

The example shown demonstrates only drift motion compensation. In the real world one will have to consider motions attributable to jitter, and perspective changes. These can significantly complicate the function that determines the relative offset positions between the sensor based detector array and the Earth surface based virtual detector array.

This approach to motion compensation cannot be utilized when motions are uncorrelated. The Earth's atmosphere is not referenced to the sensor axis nor is it exactly referenced to the Earth's surface. Thus, one must assume that atmospheric variability is not correlated. Structured cirrus coupled with its wind-induced motions are also not sufficiently correlated to be removed by this process. Likewise, contrails are not removable for the same reasons. Perspective effects and the resulting apparent motion due to the 3-dimensional nature of the topography cannot be removed unless one has detailed information about the topography. Uncorrelated motion effects will present problems for FTS spectrometers on moving platforms.

5.1 Alternative Motion Compensation Techniques

Moving the mirror at a rate that is fast compared to the rate of motion of the sensor may greatly reduce the effects induced by sensor motion. Although this conclusion is obvious, it was confirmed using the rotating chopper. Similar to the compensation techniques used by the Nimbus 4 satellite, utilization of a GSD that is large enough so that any platform or naturally induced changes in the image are too small to notice will minimize the effects of these degradations. Unfortunately, such a large field-of-view has only limited applications or utility.

6. CONCLUSIONS

Temporal effects of cirrus, contrails, drift, jitter, and possibly atmospheric irregularities can seriously affect the fidelity of data collected by an FTS spectrometer which has a small field-of-view and is operated from a moving platform. The use of FTS technology on a moving platform is a significant technical challenge. Many of the advantages of an interferometer may be negated when situated on a moving platform. Methodologies will need to be developed to determine real spectral information from artifacts. These methodologies may require other sensing techniques operating at the same time, path and GSD in order to fully understand what is real and artifact in the data.

ACKNOWLEDGEMENTS

The authors wish to thank SITAC and its sponsoring agency, the Central MASINT Organization, for allowing them to carry out this work and create this paper.

REFERENCES

1. Ackerman, S.A., *et al.*, Cloud Properties from MAS Observations during SUCCESS: Implications for MODIS, Paper presented at May 1997 AGU Meeting.
2. Ackerman, S.A., *et al.*, Retrieval of Effective Microphysical Properties of Clouds: A Wave Cloud Case Study, GRL, V 25, No. 8, pp. 1121-1124, April 15, 1998.
3. Betancor, M., Grassl, G., Grassl, H., Satellite Remote Sensing of the Optical Depth and Mean Crystal Size of Thin Cirrus and Contrails, Theor. Appl. Climatol., v. 48, pp. 101-113, 1993.
4. Dawbarn, R., Kinslow, M., Watson, D.J., Analysis of the Measured Effects of the Principal Exhaust Effluents From Solid Rocket Motors, NASA Contractor Report 3136, January 1980.

5. D.P. Duda, D.P., Spinhirne, J.D., Split Window Retrieval of Particle Size and Optical Depth in Contrails Located Above Horizontally Inhomogeneous Ice Clouds, Geophysical Research Letters, v.23, no.25, pp. 3711-3714, December 15, 1996.
6. Goodman, J., *et al.*, Shape and Size of Contrails Ice Particles, GRL, v. 25, No. 9, pp. 1327-1330, May 1, 1998.
7. Heymsfield, A.J., *et al.*, Growth of Ice Crystals in a Precipitating Contrail, GRL, v. 25, No. 9, pp. 1335-1338, May 1, 1998.
8. Jensen, E.J., *et al.*, Ice Crystal Nucleation and Growth in Contrails Forming at Low Ambient Temperatures, GRL, v. 25, No. 9, pp. 1371-1374, May 1, 1998.
9. Knollenberg, R.G., Measurements of the Growth of the Ice Budget in a Persisting Contrail, J. Atmos. Sci. v.29, No.7, pp. 1367-1374, October 1972.
10. Lawson, R.P., *et al.*, Shapes, Sizes and Light Scattering Properties of Ice Crystals in Cirrus and a Persistent Contrail During SUCCESS, GRL, v. 25, No. 9, pp. 1331-1334, May 1, 1998.
11. Minnis, P., *et al.*, Global Distribution of Contrail Radiative Forcing, GRL, v. 26, No. 13, pp. 1853-1856, July, 1, 1999.
12. Twohy, C.H., Gandrud, B.W., Electron Microscope Analysis of Residual Particles from Aircraft Contrails, GRL, v. 25, No. 9, pp. 1359-1362, May 1, 1998.
13. Van de Hulst, H.C., Light Scattering by Small Particles, John Wiley & Sons, NY, 1957.